PCCP

Accepted Manuscript

This is an Accepted Manuscript, which has been through the Royal Society of Chemistry peer review process and has been accepted for publication.

Accepted Manuscripts are published online shortly after acceptance, before technical editing, formatting and proof reading. Using this free service, authors can make their results available to the community, in citable form, before we publish the edited article. We will replace this Accepted Manuscript with the edited and formatted Advance Article as soon as it is available.

You can find more information about Accepted Manuscripts in the author guidelines.

Please note that technical editing may introduce minor changes to the text and/or graphics, which may alter content. The journal's standard Terms & Conditions and the ethical guidelines, outlined in our author and reviewer resource centre, still apply. In no event shall the Royal Society of Chemistry be held responsible for any errors or omissions in this Accepted Manuscript or any consequences arising from the use of any information it contains.

ROYAL SOCIETY OF CHEMISTRY

rsc.li/pccp

Gold-supported two-dimensional cobalt oxyhydroxide (CoOOH) and multilayer cobalt oxide islands

Jakob Fester[1], *Alex Walton*[1*], *Zheshen Li*[2] *and Jeppe V. Lauritsen*[1]

[1]Interdisciplinary Nanoscience Center (iNANO), Aarhus University, 8000 Aarhus C, Denmark

[2]ISA, Aarhus University, 8000 Aarhus C, Denmark

[*]Present address: School of Chemistry, University of Manchester, Manchester M13 9PL, UK

ABSTRACT

In the present study, we investigate the facile conversion of Co-O bilayer islands on a Au(111) surface into preferentially O-Co-O trilayers in an oxygen atmosphere and O-Co-O-Co-O multilayers at elevated temperature. We characterize and compare the island morphologies with Scanning Tunneling Microscopy, X-ray photoemission spectroscopy (XPS) and valence band spectroscopy, and show that the cobalt oxidation state changes from Co^{2+} in bilayers to purely Co^{3+} in trilayers and a mixture of Co^{2+} and Co^{3+} in the multilayer morphology. In contrast to bilayers and multilayers, the trilayer structure appears to grow pseudomorphic with the Au(111) substrate, and in addition we reveal the presence of a hydroxyl overlayer on this island type as evidenced by the appearance of a $\sqrt{3} \times \sqrt{3}R30°$ superstructure in STM correlated with the fingerprints of OH species in XPS and valence band spectroscopy. The obtained layered morphology consisting of hydroxylated trilayer islands is identical to an exfoliated sheet of the β-CoOOH which is proposed to be the active phase of the cobalt oxide oxygen evolution reaction catalyst present in the electrochemical environment, and we note that this synthesized structure thus could serve as a valuable model catalyst.

1) Introduction

Due to the high energy consumption and related environmental issues in the world of today, there is a strong interest in the construction of clean and renewable energy systems. An emerging technology to produce sustainable fuel is photo/electrochemical water splitting, i.e. generation of H_2 and O_2 from water by means of sunlight (photocatalysis) or electricity (e.g. the electrochemical cell). To meet the requirements of a large-scale production, there is a demand for effective, corrosion resistant and durable OER catalysts, of which the up-to-date best performers are oxides made from expensive noble metals such as Ir and Ru[1].

However, oxides from transition metals show potential as earth-abundant substitutes as catalysts for the OER reaction. In particular, layered double hydroxides (LDH) is a promising new class of 2D materials which is currently being investigated for OER activity, as in the case of exfoliated single layer oxyhydroxide (M-OOH) sheets of mixed Fe, Ni and Co yielding extraordinary high activities[2], even outperforming the state-of-the-art IrO_2 catalyst. Furthermore, cobalt oxides (CoO_x) have attracted considerable attention as water oxidation catalysts[3-5], and in addition to the intrinsic properties of cobalt oxides as OER catalysts, enhanced activity has been reported by synergistic effects with gold (by promotion with gold nanoparticles[6] or gold used as a substrate[7]), as well as in combination with other first-row transition metals[8-10]. Despite this progress, there is still a lack of knowledge on the detailed reaction mechanisms which at the moment represents a barrier in the development of new, improved CoO_x catalysts and other materials for the OER reaction, hence encouraging studies aiming for a fundamental understanding of these catalysts on the atomic scale.

Recently, we presented results for nanostructured cobalt oxides[11], consisting of flat, layered cobalt oxide nanoislands supported on a Au(111) substrate. For this system, the gold substrate was chosen for several reasons, most importantly: 1) The opportunity to study the synergistic effects between gold and cobalt oxides in catalysis, and 2) the chemical inertness of the flat gold surface, offering an advantage in potential future studies on structure-reactivity relationship measurements under ambient conditions or electrochemical environment. At low oxygen pressure ($\sim 1\times10^{-6}$mbar O_2) the island structure is a rocksalt Co-O bilayer exposing the (111) plane, coexisting with a minority island type comprising a wurtzite terminated Co-O-Co-O double bilayer (see the STM image in figure 6, left). Furthermore, the edge structure of these bilayer and double bilayer CoO_x islands revealed a high activity for water

dissociation at room temperature, resulting in an extraordinary degree of hydroxylation of the cobalt oxide structures[12].

Here, we explore the sensitivity of this system to elevated O_2 pressure and temperature and reveal that the island morphology and Co-O stacking is significantly influenced by these conditions. We observe two temperature- and oxygen pressure dependent phase transitions into distinct CoO_x island equilibrium morphologies in addition to the bilayer- and double bilayer structures stabilized at low oxygen pressure ($1x10^{-6}$mbar O_2) on Au(111). The two structures can be derived from the Co-O bilayers by exposure to $>1\times10^{-5}$mbar O_2 and annealing to incorporate additional oxygen, proposed to result in an O-Co-O trilayer at 400K and an O-Co-O-Co-O stacked multilayer at a higher temperature of 673K. Furthermore, we observe the existence of an ordered hydroxyl overlayer on the trilayer islands. The phases are characterized and distinguished by means of STM and X-ray photoelectron spectroscopy, providing a basis, as well as spectroscopic references, for future studies of the chemical properties of nanosized cobalt oxides on Au(111), including studies under high pressure, ambient- and aqueous conditions. We suggest that this direction could be of utmost interest, particularly due to the structural match between the presented trilayer morphology and a single layer in the β-CoOOH phase, which is reported to be the prevailing phase in liquid solution during oxygen evolution reaction.

2) Methods

2.1 Sample preparation and scanning tunneling microscopy

The experiments were performed in UHV chambers with a base pressure below 1×10^{-10}mbar, equipped with standard UHV sample preparation tools, a setup for XPS and an Aarhus STM, allowing for high-speed atomic-resolution images on a routine basis[13]. Images were acquired in the constant-current mode with the sample held at room temperature and using a tungsten tip. The optimal tunneling parameters for imaging of cobalt oxide islands on the Au(111) substrate varied to a high degree, since the contrast formation is largely determined by the STM tip configuration[14, 15]. In general, a negative tunneling bias (V_t>1000mV) and a tunneling current I_t~0.2nA was used in overview images, whereas lower bias and increased current had to be employed in high-resolution images.

A polished 6mm Au(111) single crystal was mounted on a tantalum sample holder with a thermocouple connection in close proximity to the crystal for temperature readout. A clean surface was obtained as

evaluated by XPS and STM by repeated cycles of 1.5kV Ar^+ ion sputtering and subsequent annealing at 800K for 15min. Cobalt metal was deposited with an e-beam evaporator (Oxford Applied Research, model EGCO4) in an oxygen atmosphere of always $1x10^{-6}$ mbar O_2 and a slightly elevated sample temperature of 380K. This sample temperature during cobalt deposition was found not to be of critical importance, but always kept at this value for consistency. The sample was postannealed to 523K for 15min to produce bilayer cobalt oxide islands (described in more detail in[11]) and cooled down to 300K before any measurement. Local elevated oxygen pressures at the sample surface ($>1\times10^{-5}$ mbar O_2) were reached by use of a moveable gas doser tube placed below 1mm from the gold crystal during annealing. The coverage of the resulting cobalt oxide islands (1 ML defined as the full Au(111) surface covered) was determined by STM and fixed for comparison to approximately 0.5ML or less.

2.2 X-ray photoelectron spectroscopy

Laboratory source XPS was carried out using a SPECS Phoibos 150 analyzer and Al Kα radiation (1486.6eV) from a SPECS XR 50 source operated at 350W. Survey spectra and magnification of the Au4f, Co2p and O1s regions were recorded in normal emission with respect to the detector and using a pass energy of 30eV. The acceptance spot diameter was determined to ~1mm.

Synchrotron XPS and valence band spectroscopy was performed at the AU-MATLINE endstation at the ASTRID2 synchrotron facility in Aarhus, Denmark, equipped with a Scienta electron energy analyzer and an SX-700 monochromator as well as instrumentation for Ar^+ ion sputtering and annealing for sample cleaning and preparation. All spectra were recorded in normal emission mode. For acquisition of the Au4f region a photon energy of 130eV and a pass energy of 20eV was used, O1s spectra were recorded at photon energy 665eV and pass energy of 40eV whereas the valence band region was recorded at both 50 and 110eV photon energy and a pass energy of 20eV. To estimate the amount of cobalt evaporated onto the sample, the decrease of the $Au4f_{7/2}$ surface component compared to the corresponding bulk component was monitored as function of increasing coverage of freshly synthesized cobalt oxide bilayer islands[11].

Laboratory source XPS data was energy calibrated against the $Au4f_{7/2}$ peak whereas the $Au4d_{5/2}$ component was used for energy reference in the synchrotron data. For background subtraction a

Shirley-type was employed for Co2p spectra whereas a polynomial background was used for the O1s region. The data analysis and peak fitting was performed using the IGOR Pro software (WaveMetrics).

3) Results and discussion

An overview of the synthesized cobalt oxide nanoislands that will be discussed in the following is given in figure 1. On this figure we propose the respective island structures, reflecting Co-O bilayers, O-Co-O trilayers and O-Co-O-Co-O multilayers. Starting from the well-characterized Co-O bilayer structure on Au(111)[11], the trilayer- and multilayer islands can be synthesized in sequence by annealing to 400K and 673K respectively for 3 min while dosing above 10^{-5} mbar O_2, the temperature being the critical parameter for the resulting island structure. Alternatively, the multilayer islands can be derived by direct conversion from bilayers, and both trilayers and multilayers can be synthesized directly by tuning the postanneal temperature and O_2 pressure in the original bilayer synthesis protocol described previously in[11], without the bilayer structure as an intermediate step. Hence, the three island types are equilibrium structures under the synthesis conditions and are not only determined by the kinetics during conversions in our step-by-step synthesis protocol.

3.1 Trilayers

3.1.1 Appearance in STM

We first discuss the structure of the trilayers. The appearance of trilayer islands in STM is depicted in figure 2. The apparent height is 2.9±0.1Å which is larger than the measured 1.7±0.2Å height of the bilayer islands in[11], due to the intercalation of O at the Au/oxide interface. Interestingly, this island type shows no moiré pattern as was observed on bilayers. High-resolution STM images of the basal plane of the islands (figure 2b) reveal a hexagonal atomic lattice with an interatomic spacing of a=2.8±0.1Å, whereas the precursor bilayer structure measures 3.3±0.1Å[11]. The value of 2.8Å is very close to the spacing of the underlying Au(111) of ~2.9Å, suggesting that the trilayer islands now grow pseudomorphic with the substrate, and at the same time explaining the lack of a moiré pattern. Superimposed on the atomic lattice structure in the STM image in figure 2b, patches of another hexagonal structure with a larger periodicity of 5.1±0.1Å is observed. This superstructure is most clearly seen in the more common imaging mode shown in the inset, figure 2a. Both unit cells

corresponding to the atomic lattice and the superstructure are indicated in figure 2b, revealing a rotation of 30 degree (see also the unit cells drawn on the ball model in figure 1). The superstructure is a $\sqrt{3} \times \sqrt{3}R30°$ pattern relative to the underlying cobalt oxide lattice, that results in a theoretical spacing of 5.0Å (assuming a pseudomorphic growth), being a match to the measured value. The presence of this superstructure is ascribed to a partial layer of hydroxyls for reasons that will become evident in the following. Based on the apparent height in STM and the XPS results presented in the next section, we propose that the islands consist of O-Co-O trilayers in the rocksalt structure terminated by a partial coverage of hydroxyls.

An interesting consequence of the suggested island contraction during conversion from bilayers to trilayers is shown in the STM images in figure 2c-d. These images reveal the characteristics of trilayers formed from a high coverage bilayer sample, i.e. large islands. On these islands patches of the $\sqrt{3} \times \sqrt{3}R30°$ superstructure coexist with a high density of defects and even trilayer-deep holes. We ascribe the emergence of these features to the insufficient amount of cobalt to produce a coherent trilayer island because of to the shrinkage in lattice constant from bilayer to trilayer. Instead the conversion results in the opening of pits, compensating for the lack of cobalt metal as well as the lack of mobility at this temperature (400K) to re-crystallize the structure into its equilibrium shape.

3.1.2 XPS and valence band spectroscopy

XPS gives information about oxidation states, degree of hydroxylation and differences in substrate effects for the bilayers, trilayer- and multilayer samples. Firstly, the XPS Co2p core level spectra acquired from samples consisting of bilayers, trilayers and multilayers are compared in figure 3a, showing several characteristic differences. Compared to the bilayers, both of the trilayer- and multilayer samples have a sharp main component, most pronounced in the case of trilayers. Furthermore, the shake-up satellite (SS) structure present for the bilayers is heavily suppressed and almost absent in the trilayer spectrum. The features of a broadening of the main component and a shake-up satellite are indicative of high-spin Co^{2+} species in the bilayer structure[16-18] (as also predicted by DFT calculations[11]). On the other hand, low-spin Co^{3+} compounds exhibit almost no satellite structure[19]. These observations point to the cobalt being either completely or partially in the low-spin Co^{3+} state in both of the trilayer and multilayer structures, reflecting the higher coordination to O.

The corresponding O1s core level spectra are shown in figure 3b. Here, the trilayer spectrum clearly differs from the two other cobalt oxide phases by the presence of a peak to the high binding energy (BE) side of the main component. Based on the binding energy separation of ~2eV from the main lattice component, this peak can firmly be ascribed to hydroxyls[20], a finding that is further supported by the corresponding signature of hydroxyls in the valence band spectrum at ~10eV BE[20], figure 3c. The valence band OH signature is not observed for bilayers and, surprisingly, multilayers which are derived from trilayers.

The total area of the O1s spectra (normalized to the background) reflect the relative amount of oxygen in the proposed island structures, since the spectra were acquired from the same bilayer synthesis before and after two successive conversions. The O1s peak areas of the trilayer and multilayer spectra relative to the bilayer spectrum were found to be 1.5 and 0.8 respectively. Taking into account the attenuation of photoelectron intensity through the respective island structures due to the buried O layers, these values are within uncertainties consistent with an estimate based on an electron mean free path of 5.6Å from the NIST database[21] (for 665eV photons), yielding the values 1.6 and 1.0. The oxygen content in the trilayer structure was double checked with a laboratory X-ray source (Al Kα anode), and a comparison of the normalized areas yielded a relative increase of 1.8 after conversion from bilayers to trilayers (data not shown), in agreement with the calculated factor of 1.9, using an electron mean free path of 22.4Å[21].

The valence band spectra (figure 3c) are dominated by the Au(111) substrate in the range 2-8eV BE[22]. However, near the Fermi edge differences between the three cobalt oxide phases are readily observed. It was found that the exact shape of the spectrum near the Fermi edge depended on the photon energy, but for both measurements at hv=110eV and hv=50eV, a pronounced 0.8eV BE component, in addition to one at 0.4eV, appears after conversion from bilayers to trilayers. Previous studies of Co_3O_4, that contain a mixure of Co^{2+} and Co^{3+}, have identified a peak close to 1eV BE resulting from octahedral Co^{3+} that was not present for rocksalt CoO which is purely a Co^{2+} compound. In agreement with the XPS Co2p spectra (figure 3a), this suggests that the cobalt in trilayer islands structure is in the Co^{3+} oxidation state. After the second conversion to multilayers, the Co^{3+} component is attenuated, but still easily recognized, together with a contribution from the very top of the valence band. This observation is speculated to originate from the cobalt in the multilayer structure being in two inequivalent

environments (top/bottom layer), and possibly not all of it in a well-defined Co^{3+} state. Additionally, we observe the appearance of a new component at ~1.5eV, only distinguishable in the trilayer spectrum. This peak thus serves as a fingerprint intrinsic to the trilayer structure, and we tentatively associate it with the possibility of charge transfer phenomena and final state effects[23].

Finally, the Au4f spectra for all the structures were recorded (same sample converted) and compared to the clean Au(111) sample, since it reveals information on the Au/oxide interaction. Due to the surface core level shift[24] the Au4f spectrum can be deconvoluted into two components originating from the bulk- and surface atoms respectively. After synthesis of bilayer islands on the surface, the surface component drops significantly, suggesting that the Au atoms underneath the islands lose their surface character. However, this is not observed for either trilayers or multilayers, although the amount of cobalt on the sample is the same and the apparent coverage in the case of the trilayers only slightly decreases. This interesting behavior points towards a weak interaction between the trilayer- and multilayer islands and the substrate, and could reasonably be due to the proposed incorporated layer of oxygen at the island/substrate interface, which is common to these structures.

3.1.3 Hydroxyl overlayer

To explain the observed $\sqrt{3} \times \sqrt{3}R30°$ superstructure on trilayers in STM, correlated with the clear evidence for hydroxyls in the XPS and valence band spectroscopy data only for trilayers, we propose that the O-Co-O structure is terminated by a hydroxyl overlayer. We speculate that this hydroxylation arises from a particularly high affinity of trilayers compared to bilayers and multilayers towards H_2O or H_2 dissociative adsorption, even taking place in the rest gas of UHV. This observation is in line with recently reported results on the facile hydroxylation of FeO_2 trilayers[25].

If the hydroxyls are located on the basal planes as an overlayer, it should be possible to detect a difference in the size of the OH-component in the O1s XPS spectrum relative to the total peak area by varying the surface sensitivity, i.e. the relative sensitivity between the upper- and lower oxygen layers in the trilayer structure. Therefore, a series of angle resolved XPS measurements of the O1s spectrum was performed and the results shown in figure 4a, where the intensity has been normalized to the main component of the O1s spectrum for comparison. To exclude the possibility of further hydroxylation and beam damage during the experiment, the 45 degree take-off angle (θ) data point was repeated after

the series, yielding the same result. The trend of increasing OH peak area relative to the main component correlating with larger surface sensitivity (smaller take-off angle) is qualitatively in agreement with the assumption of a hydroxyl overlayer. By fitting the spectra to two symmetric Voigt profiles it is estimated that the OH peak area increases with 18% for the 20 degree take-off angle relative to the spectrum recorded at normal incidence. A calculation based on an electron mean free path of 22.4Å in bulk CoO[21] and a Co-O layer thickness of 3Å yields 12%, however this value must be regarded as a rough estimate.

In the XPS O1s spectrum of the trilayer sample, the fitted OH component contributes with 35% of the total O1s peak area. Assuming that the intensity from the lower layer of oxygen is reduced to 82% as indicated by the laboratory X-ray source data stated earlier, the density of hydroxyl groups (in the following defined as the fraction of available basal plane lattice oxygen atoms covered) corresponds to 0.63, i.e. roughly one H atom on top of every 2 out of 3 O atoms. However, we note that the deconvolution of the O1s spectrum is likely to be more complex than the approximation used here with only two symmetric Voigt profiles, as at least three distinct oxygen species (not including edge atoms) are present in the hydroxylated trilayer islands. A distinct peak at higher BE relative to the upper lattice oxygen component has previously been encountered for O-Fe-O trilayers on Pt(111)[25] as well as in the case of a O-Rh-O trilayer on a Rh(100) surface[26]. Also, including an asymmetry with a tail towards higher binding energy, as observed for the bilayer structure (figure 3b) and also encountered for similar FeO films on Pt(111)[27], would result in a lower estimate of the OH peak area. In line with this, we instead propose the overlayer structure in figure 4b with an OH density of only 0.33 which is in agreement with the $\sqrt{3} \times \sqrt{3}R30°$ superstructure observed in STM, and results in an overall stoichiometry of $CoOOH_{0.33}$. On the other hand, we emphasize that it would not be possible to distinguish between this superstructure and the alternative ordered OH overlayer with a density of 0.66 from our STM images, since the unit cells are identical.

Also in favour of an OH density of 0.33, a superstructure with an intermediate OH density between 0.33 and 0.66 was observed on samples left in the vacuum rest gas for several hours, as shown in figure 4c. This overlayer structure (referred to as a "labyrinth" structure) is estimated to reach an OH coverage of up to 0.5 (i.e. now a total stoichiometry of $CoOOH_{0.5}$), similar to the case of our recent study of water dissociation on Co-O bilayer islands reaching saturation at exactly 50% hydroxylation

on the island basal plane[12], where the islands exhibit similar linear features in STM together with an underlying $\sqrt{3} \times \sqrt{3}R30°$ superstructure. The additional hydroxylation compared to the density of 0.33 in the OH superstructure proposed in figure 4b is likely to arise from further dissociative adsorption of H_2O or H_2 from the rest gas on the pristine islands, whereas such an additional hydroxylation would not result in a "labyrinth" structure starting from the alternative $\sqrt{3} \times \sqrt{3}R30°$ with an OH density of 0.66.

The emergence of hydroxyls on the trilayers in the first place is, as stated earlier, likewise speculated to originate from the small amount of H_2O and H_2 always present in the UHV chamber rest gas. It was found that UHV annealing of the trilayer islands did not lead to any hydroxyl desorption before the island morphology was significantly changed, a transformation already taking place at 423K. Furthermore, annealing in $4x10^{-6}$ mbar O_2 up to 523K was not observed to change the island structure, leaving the island basal plane structure unaltered. We therefore propose that the hydroxyl overlayer is an integrated part of the pristine island structure and do not elaborate on a specific hydroxylation mechanism, but rather note that it is either included in the formation mechanism or due to a very high affinity towards H_2O or H_2 dissociation. The second point of view agrees well with our observation of the labyrinth structure (figure 4, c) which appears to be originating from additional dissociative adsorption from the rest gas, as described above. The strong dissociative properties are also in line with our recently described study of the dynamics in water dissociation and hydroxylation on Co-O bilayer edges[12], however the process on trilayers leading to the initial formation of the $\sqrt{3} \times \sqrt{3}R30°$ superstructure must take place at a much faster rate.

The trilayer islands reported here show strong similarities with structures formed by oxidation of FeO thin films on both Pd(111) and Pt(111), which have been studied and described in a number of previous publications[28-30], however with several notable differences. On both Pt(111) and Pd(111) the formation of an O-Fe-O trilayer takes place in specific domains of the moiré structure, and hence does not convert the complete metal oxide sheet, as we observe for cobalt oxide on Au(111). As found in the present study, a $\sqrt{3}\,x\sqrt{3}R30°$ superstructure was also observed on the oxidized patches of the film on Pt(111), recently ascribed to the presence of hydroxyls based on XPS measurements[25]. Our observation that a coherent O-Co-O trilayer with a $\sqrt{3}\,x\sqrt{3}R30°$ superstructure covers the complete structure might be associated with the "island" nature of the reported trilayers, as opposed to the case of a closed

monolayer film. Along this line, we speculate that the process of converting the complete structure into one preferred domain type could be favored in the "island" morphology, which in this case allows for an easier release of stress and strain.

Finally, we address the reason for the apparent pseudomorphic growth of the trilayer structure on Au(111), which is surprising in relation to the in-plane expansion of the cobalt oxide lattice for both bilayers and multilayers, leading to the emergence of a moiré pattern in these cases. Common to bilayers and multilayers is the termination by a Co-O repeat unit, formally resulting in an unfavorable dipole moment. It is known from other systems, including CoO- and FeO on Pt(111) as well as graphite-like ZnO bilayer films on Au(111)[31-33], that such a polarization can be compensated by a mechanism pulling the positively and negatively charged metal and oxygen layers closer together, accounting for the observed lateral expansion. We suggest that the positively charged overlayer of hydroxyls on the trilayer structure is itself providing a compensation mechanism, making this expansion less crucial for the island stability. Moreover, the in-plane hexagonal unit-mesh length in ordered layers of hydroxylated β-CoOOH was reported to be only 2.851Å[34, 35] which is lower than the corresponding value for bulk rocksalt-type CoO of 3.012Å[36] and hence closer to the atomic periodicity on Au(111) (2.884Å).

3.2 Multilayers

Annealing to an elevated temperature of 673K for 3 min in the same oxygen atmosphere as used in the trilayer synthesis ($>1\times10^{-5}$mbar O_2) results in a further phase transition into islands with a stacked morphology (figure 5) and a distinctly different top facet appearance in STM. The apparent height is now 4.8±0.2Å, but a minority (~10%) of the islands exhibit only 2.6±0.2Å. As the height difference of 2.2±0.3Å agrees well with the Au(111) step height of 2.4Å and because of the similar appearance, the lower minority islands are interpreted as the same structure buried one layer into the Au(111) substrate (figure 5d), a finding that we ascribe to the high mobility of Au at the elevated multilayer formation temperature of 673K. The high density of the minority species along Au(111) step edges (figure 5a) furthermore supports this model. Again the basal planes are imaged as a hexagonal lattice of atoms, with expanded interatomic spacing relative to the Au(111) of 3.3±0.1Å, and the mismatch of 13.9% is

the origin of the emergence of an ordered and very corrugated moiré pattern always visible on this island type (see figures 5a and 6). Taking the measured height into account together with the atomic arrangement on the basal planes, we conclude that the structural model in figure 1, consisting of 5 stacked layers (O-Co-O-Co-O), referred to as a "multilayer" structure, is the best match.

Changes in the cobalt oxide island apparent coverage (in the following defined in terms of the percentage of Au(111) surface area covered) after the series of conversions sketched in figure 1 also support the hypothesized structures, since the apparent coverage reflects the cobalt density (number of cobalt atoms per island area) in the different island types. The apparent coverage was determined from a large number of STM images taken on the same sample, starting with the bilayer structure (figure 6, left) followed by conversion to trilayers (middle) and in a second step further conversion to multilayers (right). The relative apparent coverage (θ_{rel}) decreased only slightly from 100% to 89±4% of the original after conversion to trilayers, but significantly to 53±2% for the multilayers, i.e. about half of the initial apparent coverage. As the proposed multilayer structure comprises two layers of cobalt relative to only one layer in the original bilayers, the observation of roughly half coverage after conversion supports the structural model. In the case of trilayers, a contraction is indeed expected due to the decrease in unit cell area to ~80% relative to the Bilayer structure (assuming a lattice parameter of 3.3Å for bilayers[11]), accounting for the initial drop in apparent coverage. These considerations are, however, ignoring the small amount of double bilayers (described in[11]) present on the sample in figure 6, which are assumed to convert directly into multilayers already after first conversion (figure 6, middle). To take this into account, the total amount of cobalt in terms of monolayer equivalents (1 monolayer equivalent (MLE) being the number of Au(111) surface atoms) based on the hypothesized island structures was estimated. The outcome of this calculation was 0.39±0.02MLE, 0.38±0.02MLE and 0.35±0.02MLE indicating that the amount of cobalt stays roughly constant as expected (however, at elevated temperature metallic cobalt could alloy into the bulk of the Au crystal and possibly account for the slight decrease[37]).

An alternative to the proposed multilayer structure is the hexagonal termination of spinel Co_3O_4. Indeed, cobalt oxide islands on Au(111) with a similar appearance in STM to the multilayers presented here were recently suggested to be the Co_3O_4[38]. This is an obvious candidate since the repeat unit

distance of 4.667Å closely matches the measured height. Also, the evidence of Co^{3+} species in the XPS and valence band spectroscopy data is expected for spinel Co_3O_4. However, although the possibility of Co_3O_4 cannot be completely excluded, we argue that the multilayer structure reported here is in better agreement with our observations for several reasons: 1) The interatomic spacing of the basal plane measured by STM yielding 3.3±0.1Å implies a large expansion of 16% relative to the oxygen spacing of 2.885Å in bulk Co_3O_4. 2) The expected periodicity of 5.7Å in the hexagonal mesh of $Co_3O_4(111)$ due to the arrangement of the cobalt cations was never observed on multilayers. In contrast, this was previously reported in STM studies of both Co_3O_4 films on Ir(100)[39] and Fe_3O_4 on Pt(111)[32]. 3) Finally, the lower density of cobalt per area in Co_3O_4 islands compared to the Multilayer structure would result in a decrease in apparent coverage after conversion from bilayers down to 66%, whereas we observe only 53%. Recently, multilayer islands synthesized at elevated O_2 pressure similar to the ones we propose here have been reported on Ag(100), consisting of close packet FeO(111), estimated to comprise three Fe layers and to be terminated by oxygen layers at both the Ag(100) and vacuum interfaces[40].

3.3 Relevance of the trilayer and multilayer structures

Finally, we address the relevance of the synthesized structures in relation to the group of emerging cobalt oxide catalyst materials for the OER reaction. We firstly note, that our reported bilayers, trilayers and multilayers all display the general morphology of a 2D sheet with Co and O stacked in layers, in common with the reported OER cobalt oxide catalysts under operating conditions[2, 7, 41]. This provides a well-characterized platform to study a selection of catalytically relevant atomic sites located at the island edges, which are believed to host the active site for the OER reaction[2]. The chemical inertness of the gold substrate furthermore enables potential electrochemical studies as well as extended studies to elevated/ambient gas pressures and liquid environment.

Secondly, we note that the trilayer morphology precisely reflects the structure of a single layer in the β-CoOOH catalyst phase. As pointed out earlier, these structures display matching lattice parameters, and contain the same O-Co-O sandwich morphology as well as the presence of hydroxyls. Interestingly, the stoichiometry in the labyrinth structure observed here is even exactly matching the recently reported

$H_{0.5}CoO_2$, suggested by theoretical simulations of *in situ* high-resolution X-ray absorption spectroscopy data[34] of a cobalt oxide/Au(111) catalyst under OER operating conditions. On the other hand, the hydroxylation restricted to only the vacuum side oxygen layer on the trilayers and the presence of the Au substrate is notable differences from free standing sheets of β-CoOOH, however the interaction with the Au surface appears to be weak according to our XPS data (section 3.1.2).

Conclusions

In summary, we report two oxygen pressure- and temperature induced phase transitions between Co-O bilayers on Au(111) into oxygen-rich phases synthesized by exposure to > 1×10^{-5}mbar O_2 and consisting of rocksalt-type O-Co-O trilayers (at 423K) and O-Co-O-Co-O multilayers (at 673K) respectively. We characterized these phases by means of STM and XPS to investigate the atomic structure and cobalt oxidation states. Cobalt changes from Co^{2+} in bilayers to pure Co^{3+} in trilayers and mixed valencies with a high proportion of Co^{3+} in multilayers. In the $Au4f_{7/2}$ XPS spectrum, the lack of a suppressed surface component as observed for bilayers indicates a weak island-to-substrate binding which is ascribed to the interface oxygen atoms in both structures. Trilayers grow pseudomorphically on the Au(111) surface and are, surprisingly, terminated by a hydroxyl overlayer, as indicated by OH components in the O1s XPS spectrum and valence band. In addition, a series of angle-resolved XPS measurements confirmed that the hydroxyls are located on the top basal plane. The presence of a hydroxyl overlayer further explains the observed $\sqrt{3} \times \sqrt{3}R30°$ superstructure on trilayers in STM. On the other hand, multilayers show no evidence for hydroxyls and display the same interatomic expansion relative to bulk rocksalt CoO as bilayers. Finally, we note that the reported structures could be highly relevant as a model system for investigations of water splitting cobalt oxide catalysts, based on the strong resemblance in structure and stoichiometry of, especially, the trilayer islands with a sheet of the layered β-CoOOH structure which has been reported to be the prevailing cobalt oxide phase during operation in electrochemical environment.

Acknowledgement

The Lundbeck Foundation is acknowledged for financial support. We also acknowledge beamtime on the AU-Matline of the ASTRID2 synchrotron, Aarhus, Denmark.

Figures

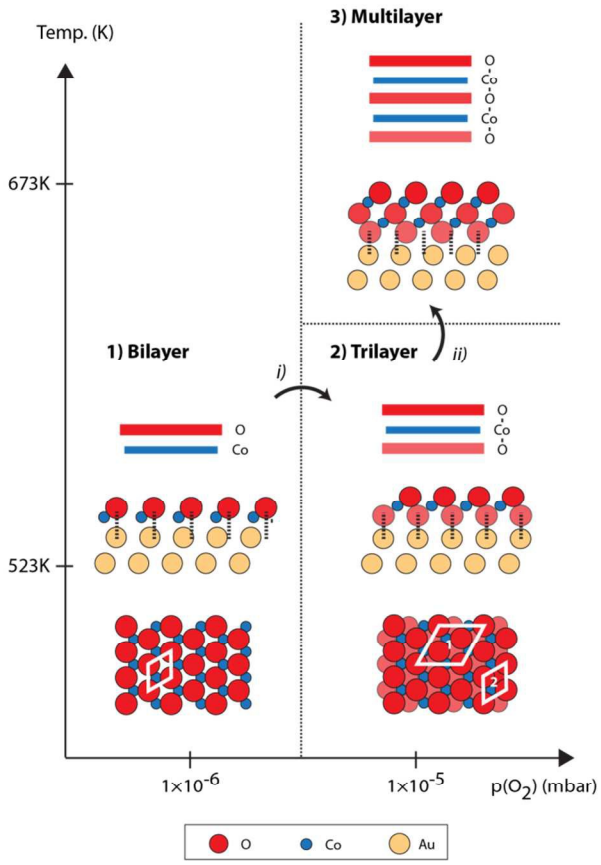

Figure 1

Synthesis conditions and schematic phase diagram for layered Co oxide structure on Au(111) as a function of preparation conditions. Ball models are shown in topview and side view for: 1) Rocksalt CoO(111)/Au(111) bilayer islands, 2) trilayer islands and 3) multilayer islands. Vertical dotted lines in the ball models indicate whether the respective CoO_x lattices are expanded relative to the underlying Au(111) or not. The arrows marked *i)* and *ii)* show a sequential experimental synthesis procedure by conversions starting from the bilayer morphology. The white rhombuses 1 and 2 show the two unit cells observed in STM (see figure 2).

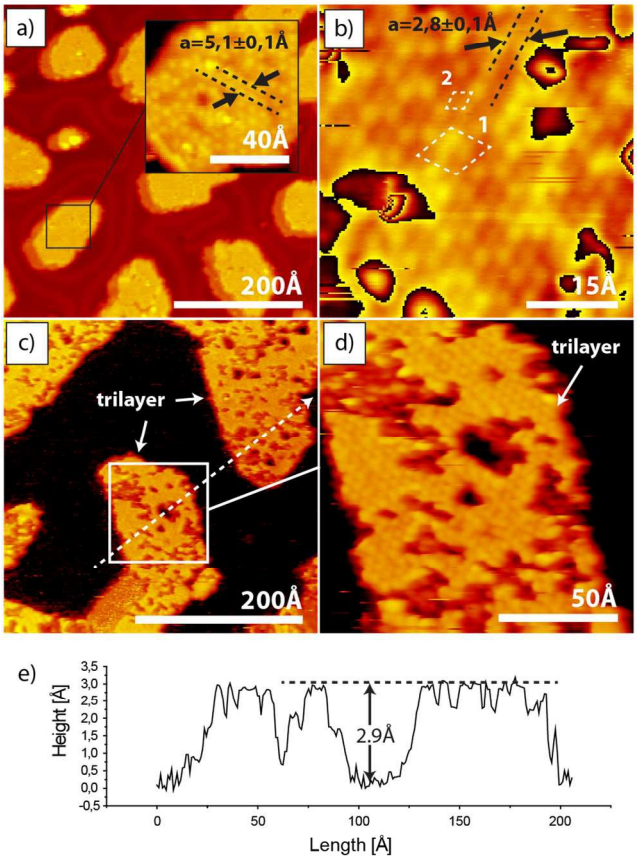

Figure 2

Cobalt oxide trilayers on Au(111). (a) Overview STM image (-1.23V, 0.3nA) of a trilayer sample. Inset: Trilayer basal plane in the most common imaging mode, indicating a hexagonal ordering with a periodicity and rotation in agreement with a $\sqrt{3} \times \sqrt{3}R30°$ superstructure. (b) STM image (-0.613V, -0.3nA, cyclic color scale) of the trilayer basal plane in a rare imaging mode revealing both of the two characteristic unit cells (also indicated on the ball model in figure 1). (c-d) STM images (0.132V, 0.3nA) of trilayer islands formed by conversion from a high-coverage bilayer sample (island coverage ~50% of total Au(111) area) with a high density of pits in the basal planes. (e) Height profile corresponding to the dotted line in c).

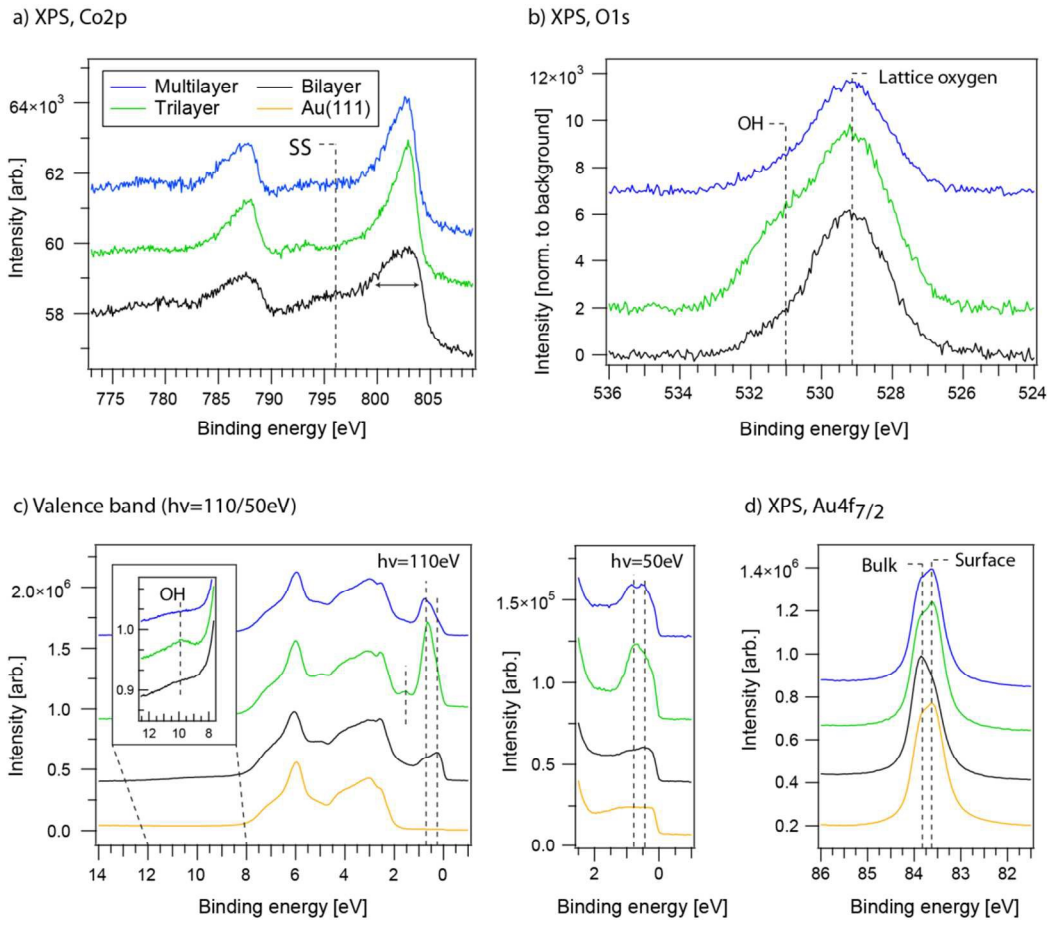

Figure 3

(a) Co2p XPS spectra of bilayer-, trilayer- and multilayer CoO_x/Au(111) samples (Al Kα source, 1486.6eV). SS=shake up satellite structure. (b-d) Synchrotron XPS and valence band spectroscopy data. (b) O1s, 665eV photon energy. (c) Valence band, 110eV/50eV photon energy. Vertical lines mark distinguishable components near the Fermi edge. (d) $Au4f_{7/2}$, 130eV photon energy. Differences in the relative intensity between the bulk- and surface core level shift components are indicated by vertical lines.

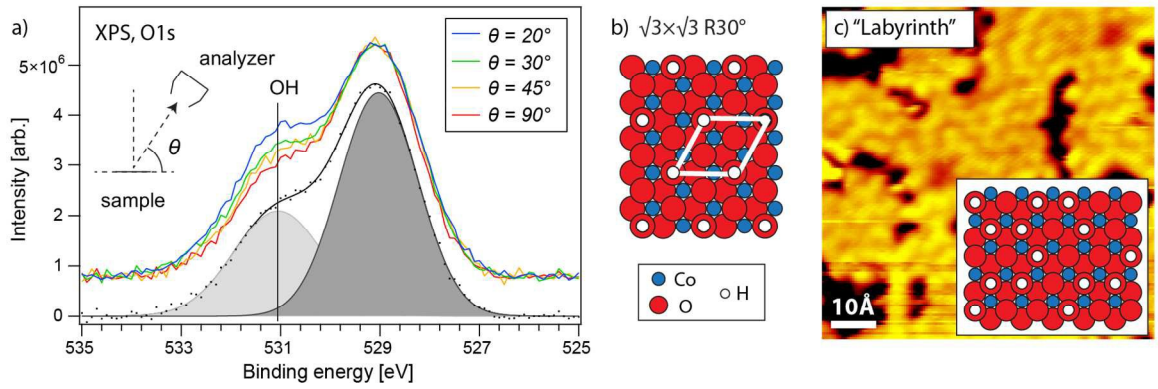

Figure 4

(a): Angle resolved XPS measurements of the O1s core level in trilayer islands on Au(111) (Al Kα source, 1486.6eV). The intensity of the spectra was normalized to the main component. θ is the take-off angle as defined on the inset. (b) Proposed structure of a hydroxyl overlayer on trilayer islands corresponding to a $\sqrt{3} \times \sqrt{3}R30°$ pattern. (c) STM image (0.105V, 0.5nA) showing a "Labyrinth" overlayer structure observed on samples left in the UHV rest gas for several hours (same sample as the pristine synthesis shown in figure 2c-d). Inset: Suggested hydroxyl superstructure reaching an OH density of 0.5).

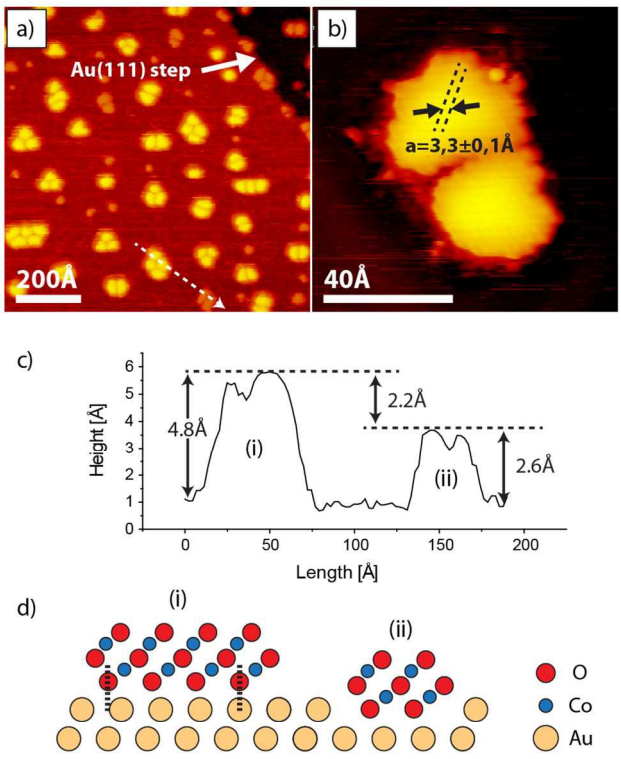

Figure 5

Cobalt oxide multilayers on Au(111). (a) Overview STM image (-0.884V, 0.3nA) of a typical multilayer sample showing islands with two characteristic heights with the low-type minority (~10%) proposed to be buried multilayers as sketched in (d, ii). (b) High-resolution STM image (-0.625V, 0.4nA) of a multilayer island revealing the hexagonal basal plane atomic lattice. (c) Height profile corresponding to the dotted line in a). d) Structural model of multilayer and buried multilayer.

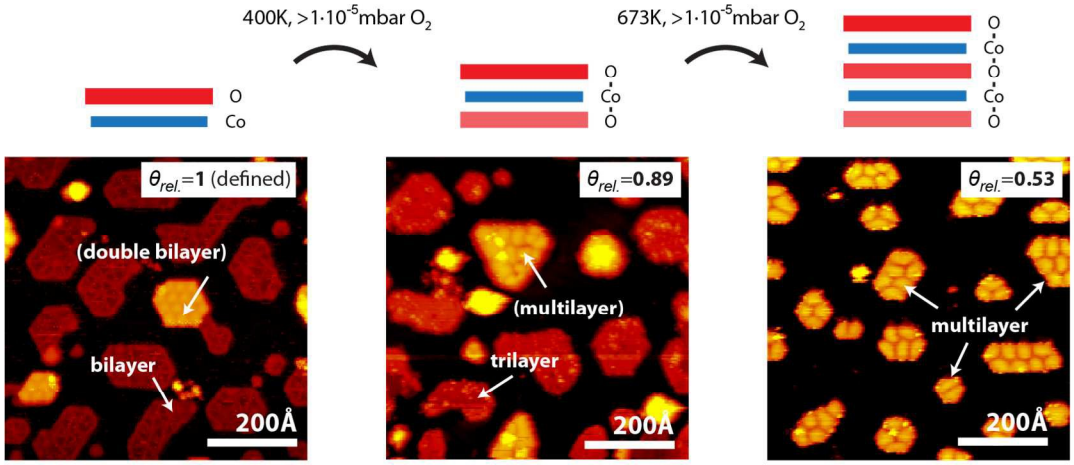

Figure 6

Coverage analysis from images acquired from the same sample, exploiting a sequential synthesis protocol by conversion of bilayers into trilayers and further into multilayers. (STM images: a) I_t=-0.240nA, V_t=-1250.0mV, b) I_t=-0.200nA, V_t=-1238.7mV, c) I_t=-0.200nA, V_t=-1486.5mV).

References

1. J. Cheng, H. Zhang, G. Chen and Y. Zhang, *Electrochimica Acta*, 2009, **54**, 6250-6256.
2. F. Song and X. Hu, *Nature communications*, 2014, **5**.
3. X. Deng and H. Tüysüz, *ACS Catalysis*, 2014, **4**, 3701-3714.
4. J. Rosen, G. S. Hutchings and F. Jiao, *Journal of the American Chemical Society*, 2013, **135**, 4516-4521.
5. L. Liao, Q. Zhang, Z. Su, Z. Zhao, Y. Wang, Y. Li, X. Lu, D. Wei, G. Feng and Q. Yu, *Nature nanotechnology*, 2014, **9**, 69-73.
6. X. Lu, Y. H. Ng and C. Zhao, *ChemSusChem*, 2014, **7**, 82-86.
7. B. S. Yeo and A. T. Bell, *Journal of the American Chemical Society*, 2011, **133**, 5587-5593.
8. M. G. De Chialvo and A. Chialvo, *Electrochimica acta*, 1993, **38**, 2247-2252.
9. M. Bajdich, M. n. García-Mota, A. Vojvodic, J. K. Nørskov and A. T. Bell, *Journal of the American chemical Society*, 2013, **135**, 13521-13530.
10. G. Wu, N. Li, D.-R. Zhou, K. Mitsuo and B.-Q. Xu, *Journal of Solid State Chemistry*, 2004, **177**, 3682-3692.
11. A. S. Walton, J. Fester, M. Bajdich, M. A. Arman, J. Osiecki, J. Knudsen, A. Vojvodic and J. V. Lauritsen, *ACS nano*, 2015, **9**, 2445-2453.
12. J. Fester, G. M. Melchor, A. S. Walton, M. Bajdich, Z. Li, L. Lammich, A. Vojvodic and J. V. Lauritsen, *Nature communications*, *accepted*.
13. F. Besenbacher, E. Lægsgaard, K. Mortensen, U. Nielsen and I. Stensgaard, *Review of scientific instruments*, 1988, **59**, 1035-1038.
14. L. R. Merte, L. C. Grabow, G. Peng, J. Knudsen, H. Zeuthen, W. Kudernatsch, S. Porsgaard, E. Lægsgaard, M. Mavrikakis and F. Besenbacher, *The Journal of Physical Chemistry C*, 2011, **115**, 2089-2099.
15. H. Monig, M. Todorovic, M. Z. Baykara, T. C. Schwendemann, L. Rodrigo, E. I. Altman, R. Perez and U. D. Schwarz, *ACS nano*, 2013, **7**, 10233-10244.
16. N. McIntyre and M. Cook, *Analytical Chemistry*, 1975, **47**, 2208-2213.
17. T. Chuang, C. Brundle and D. Rice, *Surface Science*, 1976, **59**, 413-429.

18. D. Gallant, M. Pezolet and S. Simard, *The Journal of Physical Chemistry B*, 2006, **110**, 6871-6880.
19. D. Barreca, A. Gasparotto, O. I. Lebedev, C. Maccato, A. Pozza, E. Tondello, S. Turner and G. Van Tendeloo, *CrystEngComm*, 2010, **12**, 2185-2197.
20. M. A. Henderson, *Surface Science Reports*, 2002, **46**, 1-308.
21. *NIST Electron Inelastic-Mean-Free-Path Database*, **http://www.nist.gov/srd/nist71.cfm**, accessed October 2015.
22. J. Stöhr, G. Apai, P. Wehner, F. McFeely, R. Williams and D. Shirley, *Physical Review B*, 1976, **14**, 5144.
23. L. Giordano, G. Pacchioni, C. Noguera and J. Goniakowski, *Topics in Catalysis*, 2013, **56**, 1074-1081.
24. P. Heimann, J. Van der Veen and D. Eastman, *Solid State Communications*, 1981, **38**, 595-598.
25. N. Johansson, L. R. Merte, E. Grånäs, S. Wendt, J. N. Andersen, J. Schnadt and J. Knudsen, *Topics in Catalysis*, 2016, 1-10.
26. J. Gustafson, A. Mikkelsen, M. Borg, J. N. Andersen, E. Lundgren, C. Klein, W. Hofer, M. Schmid, P. Varga and L. Köhler, *Physical Review B*, 2005, **71**, 115442.
27. J. Knudsen, L. R. Merte, L. C. Grabow, F. M. Eichhorn, S. Porsgaard, H. Zeuthen, R. T. Vang, E. Lægsgaard, M. Mavrikakis and F. Besenbacher, *Surface Science*, 2010, **604**, 11-20.
28. H. Zeuthen, W. Kudernatsch, G. Peng, L. R. Merte, L. K. Ono, L. Lammich, Y. Bai, L. C. Grabow, M. Mavrikakis and S. Wendt, *The Journal of Physical Chemistry C*, 2013, **117**, 15155-15163.
29. L. Giordano, M. Lewandowski, I. Groot, Y.-N. Sun, J. Goniakowski, C. Noguera, S. Shaikhutdinov, G. Pacchioni and H.-J. Freund, *Journal of Physical Chemistry C*, 2010, **114**, 21504-21509.
30. Y.-N. Sun, Z.-H. Qin, M. Lewandowski, E. Carrasco, M. Sterrer, S. Shaikhutdinov and H.-J. Freund, *Journal of Catalysis*, 2009, **266**, 359-368.
31. M. De Santis, A. Buchsbaum, P. Varga and M. Schmid, *Physical Review B*, 2011, **84**, 125430.
32. W. Weiss and W. Ranke, *Progress in Surface Science*, 2002, **70**, 1-151.
33. X. Deng, K. Yao, K. Sun, W.-X. Li, J. Lee and C. Matranga, *The Journal of Physical Chemistry C*, 2013, **117**, 11211-11218.

34. D. Friebel, M. Bajdich, B. S. Yeo, M. W. Louie, D. J. Miller, H. S. Casalongue, F. Mbuga, T.-C. Weng, D. Nordlund and D. Sokaras, *Physical Chemistry Chemical Physics*, 2013, **15**, 17460-17467.
35. R. G. Delaplane, J. A. Ibers, J. R. Ferraro and J. J. Rush, *The Journal of Chemical Physics*, 1969, **50**, 1920-1927.
36. W. Meyer, D. Hock, K. Biedermann, M. Gubo, S. Müller, L. Hammer and K. Heinz, *Physical review letters*, 2008, **101**, 016103.
37. H. Okamoto and T. B. Massalski, *Phase diagrams of binary gold alloys*, ASM International, 1987.
38. M. Li and E. Altman, *Surface Science*, 2014, **619**, L6-L10.
39. K. Heinz and L. Hammer, *Journal of Physics: Condensed Matter*, 2013, **25**, 173001.
40. L. R. Merte, M. Shipilin, S. Ataran, S. Blomberg, C. Zhang, A. Mikkelsen, J. Gustafson and E. Lundgren, *The Journal of Physical Chemistry C*, 2015, **119**, 2572-2582.
41. R. Subbaraman, D. Tripkovic, K.-C. Chang, D. Strmcnik, A. P. Paulikas, P. Hirunsit, M. Chan, J. Greeley, V. Stamenkovic and N. M. Markovic, *Nature materials*, 2012, **11**, 550-557.